THE JOURNAL OF PHYSICAL CHEMISTRY LETTERS
A JOURNAL OF THE AMERICAN CHEMICAL SOCIETY

pubs.acs.org/JPCL Letter

Prediction of Multiple Hydrogen Ligation at a Vanadium(II) Site in a Metal−Organic Framework

Romit Chakraborty,* Kurtis M. Carsch, David E. Jaramillo, Yuto Yabuuchi, Hiroyasu Furukawa, Jeffrey R. Long, and Martin Head-Gordon*

Cite This: J. Phys. Chem. Lett. 2022, 13, 10471−10478 Read Online

ACCESS | Metrics & More | Article Recommendations | Supporting Information

ABSTRACT: Densifying hydrogen in a metal−organic framework (MOF) at moderate pressures can circumvent challenges associated with high-pressure compression. The highly tunable structural and chemical composition in MOFs affords vast possibilities to optimize binding interactions. At the heart of this search are the nanoscale characteristics of molecular adsorption at the binding site(s). Using density functional theory (DFT) to model binding interactions of hydrogen to the exposed metal site of cation-exchanged MFU-4*l*, we predict multiple hydrogen ligation of H_2 at the first coordination sphere of V(II) in V(II)-exchanged MFU-4*l*. We find that the strength of this binding between the metal site and H_2 molecules can be tuned by altering the halide counterion adjacent to the metal site and that the fluoride containing node affords the most favorable interactions for high-density H_2 storage. Using energy decomposition analysis, we delineate electronic contributions that enable multiple hydrogen ligation and demonstrate its benefits for hydrogen adsorption and release at modest pressures.

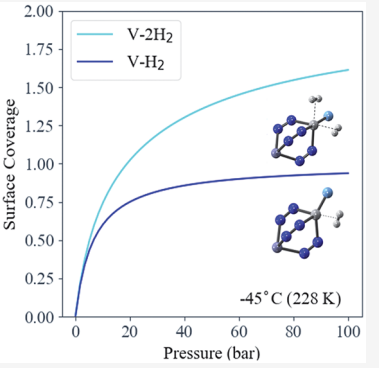

A major challenge for a future hydrogen-based economy is the need for energy intensive compression and liquefaction of H_2 to counteract its low volumetric energy density.[1,2] Current machinery for hydrogen distribution for vehicular storage involves compression above 350 bar,[3] where the majority of the operating cost at the refuelling station is due to the compressor.[4] In addition to environmental and energy costs of such high-pressure treatment, storage of a highly compressed flammable gas is a safety concern for vehicle operators. Metal−organic frameworks (MOFs) offer a potential solution to this problem as a broad class of new materials that can, if appropriately designed, adsorb and release H_2 at more moderate pressures.[5]

As a materials design problem, optimization of MOFs for hydrogen storage is an enormous challenge, with a complex interplay between constraints imposed by the desired functional characteristics and nontrivial synthetic considerations. The high surface to volume ratio in a MOF combined with its structural and chemical tunability results in combinatorial numbers of possibilities for the design of an optimal storage material.[5,6] Nonetheless, the syntheses and measurements of new MOF combinations are time-consuming and resource-intensive, prompting the need for computationally aided approaches. Reliable quantum chemical calculations can screen candidate materials to identify promising leads, at a minimum. Design principles for high-density hydrogen storage can also be derived from computational prediction of the electronic structure of hydrogen interacting with the MOF binding site and the associated pore.[7] In-silico characterizations of the feature space in MOFs can identify the leading contributors to interactions and thereby offer a pathway to release H_2 below operating pressures of 100 bar.

In the list of technical targets for vehicular storage, the US Department of Energy (DOE) has earmarked volumetric storage capacity at 40 g/L by the year 2025 at operating conditions in the range of [−40, 60] °C and 5 to 100 bar.[7] The current record for physisorptive storage is held by Ni_2(*m*-dobdc) (*m*-dobdc^{4-} = 4,6-dioxido-1,3-benzenedicarboxylate) with a volumetric capacity of 11 g/L at 25 °C for a pressure swing between 100 and 5 bar.[8] Evidently, physisorption-driven storage alone does not suffice for room temperature storage applications, and stronger binding interactions are desirable.[5,6,9,10] Given the demand for high-density storage of hydrogen in the solid state,[11,12] it is highly desirable to bind *multiple* hydrogens at an open metal site in a MOF with binding enthalpies in the −15 to −25 kJ/mol range though this has not yet been demonstrated. Indeed there have been very few demonstrations of multiple H_2 binding at any potentially realistic site.[13−16] Strong H_2-binding to a five-coordinate V(II) center in $V_2Cl_{2.8}$(btdd), which displays an isosteric heat of 21 kJ/mol,[17] provides promise for ambient temperature storage of hydrogen. Guided by this insight, we wanted to explore

Received: September 16, 2022
Accepted: October 31, 2022
Published: November 3, 2022

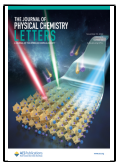

https://doi.org/10.1021/acs.jpclett.2c02844
J. Phys. Chem. Lett. 2022, 13, 10471−10478

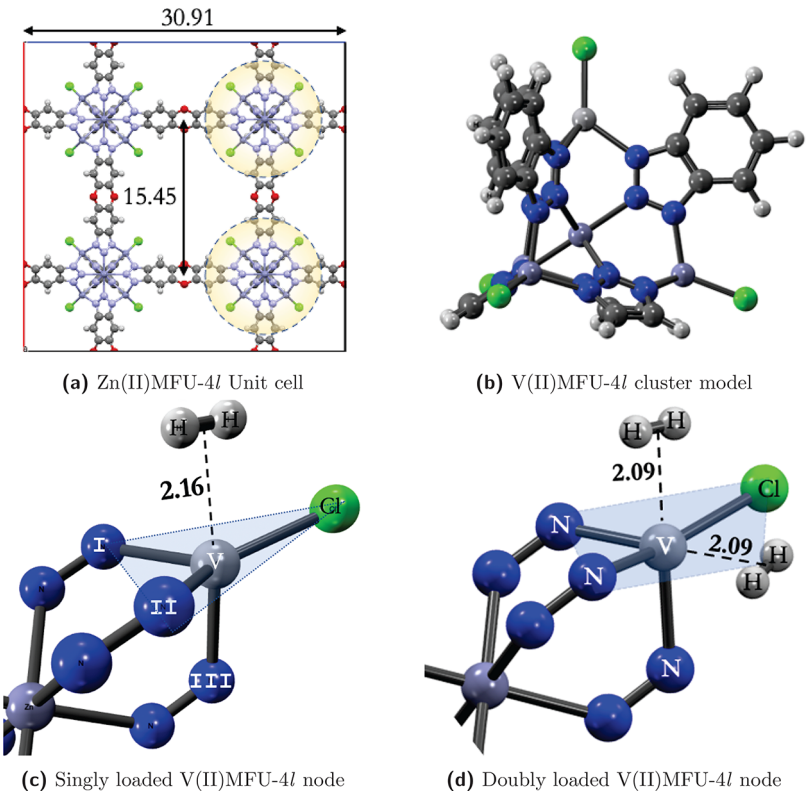

(a) Zn(II)MFU-4*l* Unit cell (b) V(II)MFU-4*l* cluster model

(c) Singly loaded V(II)MFU-4*l* node (d) Doubly loaded V(II)MFU-4*l* node

Figure 1. (a) Cubic cell unit of Zn(II)MFU-4*l*, the parent material for the transmetalated V(II)MFU-4*l* studied here. (b) Cluster model for V(II)MFU-4*l* with Cl^- ions. Parts (c) and (d) are close-up views of the equilibrium geometries of singly and doubly loaded V(II)MFU-4*l*. Vanadium sites are rendered in gray, nitrogen in blue, chloride in green, and Zn in violet gray. Distances are labeled in Å.

analogous H_2 binding to V(II) in a four-coordinate scaffold with two available coordination sites, which could potentially be accessed within MFU-4*l*. Toward this objective, we predict feasible ligation of two hydrogen molecules to V(II) in V(II)-exchanged MFU-4*l* which has been previously prepared and characterized in a hydrated form.[18] Furthermore, the parent material, MFU-4*l*, has the benefit of being able to readily tune the peripheral anion, which can modulate the binding energetics of H_2. Adsorption behavior that is controlled by primary coordination sphere anions has been demonstrated recently in the metal−organic-framework Ni_2X_2(btdd).[19]

The parent MFU-4*l* framework is highly robust and demonstrates exceptional thermal stability.[20,21] The defining feature of MFU-4*l* is scorpionate-type coordination with $BTDD^{2-}$ ligands (H_2BTDD = bis(1*H*-1,2,3-triazolo[4,5-*b*],[4′,5′-*i*])dibenzo[1,4]dioxin) at these tetrahedral metal sites, where a tridentate ligand speared with nitrogens binds the metal in a *fac* manner. The term scorpionate[22] derives from two donor sites grasping at the metal like the pincers of a scorpion followed by a third and final donor, the stinger, reaching over the plane formed by the metal site and the two donors. The peripheral Zn(II) ions in MFU-4*l* can be exchanged for a variety of transition metal divalent cations.[18,23−26] This material piqued our interest for two reasons: (i) it features 4 outer metal sites per node that have tetrahedral coordination, and (ii) metal-exchange for V(II), which is known to favor octahedral coordination, has been reported[18] for these sites. Figure 1a shows the cubic unit cell of Zn(II)MFU-4*l*. Here we consider each node to behave independently. The pentanuclear cluster model shown in Figure 1b was built from the parent scaffold. The binding environment around the V(II) site was modeled by truncation of the node at its benzotriazolate extremities, and a triazolate truncation of the linker was employed elsewhere, giving a molecular formula of $V(II)_1Zn(II)_4Cl_4(btz)_3(tz)_3$ (btz^- = benzotriazolate, tz^- = triazolate) to the cluster. An octahedral Zn(II) at the center of the node is surrounded by 4 peripheral tetrahedral sites, one of which is substituted with V(II). Following experimental characterization of H_2 binding to V(II) in a similar ligand-field environment in $V_2Cl_{2.8}$(btdd),[17] we model V(II) in its high-spin (S = 3/2) ground state.

The MOF crystal is periodic and three-dimensional, and upon approach of a guest molecule to a metal site, there may be strong binding contributions reflecting local chemical interactions at the site, supplemented by weaker long-range dispersion interactions. To ensure accurate description of the critical local chemistry, we employ the ωB97M-V functional,[27] which is an accurate range-separated hybrid metaGGA that includes nonlocal VV10 dispersion,[28] designed by the combinatorial "survival of the most transferable" protocol. ωB97M-V was the top-performing hybrid density functional in several large assessments, including the MGC84 database,[29] the large and diverse GMTKN55 benchmark data set,[30−32] and the TMC151 transition metal database.[33] These findings are buttressed by a recent extensive benchmark[34,35] of density functionals for hydrogen storage. Employing ωB97M-V limits calculations to a cluster node, as exact exchange is not feasible for periodic calculations. We have chosen our cluster model to be very faithful to the full MOF for capturing metal−ligand interactions at short distances and to be adequate for capturing the leading contributions from comparatively long-range dispersion forces that prevail in MOF pores. Geometries

https://doi.org/10.1021/acs.jpclett.2c02844
J. Phys. Chem. Lett. 2022, 13, 10471−10478

E(kJ/mol)	V(II)L_3Cl-H_2	V(II)L_3ClH_2-H_2	ΔΔ
Δ Prep	8.8	11.1	2.3
Δ Frz	19.8	18.3	**-1.5**
Δ Pol	-11.9	-13.9	**-2.0**
Δ CT	-30.0	-32.8	**-2.8**
Δ H_2→V(II)	-23.4	-26.1	**-2.7**
Δ V(II)→H_2	-6.6	-6.7	**-0.1**
Δ E	-13.3	-17.3	**-4.0**

(a)

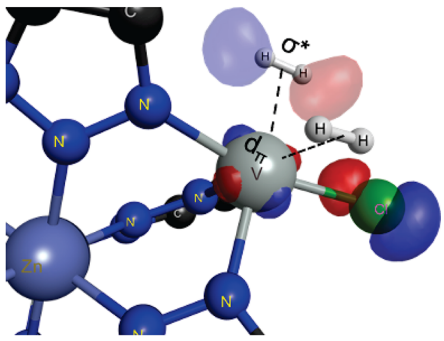

(b)

Figure 2. (a) Comparison of energy decomposition of the first and second H_2 binding to V(II)(Cl)MFU-4*l*. Cooperative binding of H_2 to V(II) in MFU-4*l* is predicted by the increase in binding energy on adsorption of the second hydrogen. (b) Complementary occupied-virtual pair (COVP) of charge transfer orbitals for backdonation from V(II) to the second ligated H_2.

were optimized in the def2-SVP basis that contains *f* polarization at the transition metal site and *p* polarization at the hydrogens. The def2-ECP effective core potential was used for elements heavier than Rb ($Z = 37$), such as iodine.[36] Single point calculations were performed with this basis augmented with the fairly large Karlsruhe def2-TZVPPD basis[37,38] in the binding region with 2*f* and 1*g* polarization functions at the metal site and 3*p* and 1*d* polarization functions for hydrogen. Geometries were converged to 3×10^{-4} kJ/mol in energy, and 3×10^{-5} au in the maximum gradient component. Counterpoise corrections proposed by Boys and Bernardi[39] were employed to reduce basis set superposition error (BSSE) in energy evaluations.

Figures 1c and d show close-ups of equilibrium geometries for single and double hydrogen loaded V(II)MFU-4*l* nodes, with Cl^- ions. The second hydrogen binds closer to the metal site with a center of mass distance of 2.09 Å (the first H_2 binds at 2.16 Å). The singly loaded node assumes a distorted trigonal bipyramidal configuration around the V(II) site (see Figure 1c) with the equatorial plane formed by the chloride ion and nitrogens I and II and with the axial sites occupied by hydrogen and nitrogen III. The axial H_2 and N_{III} make angles of 90.6° and 91.3° with the equatorial N_{II}. The doubly loaded node forms a distorted octahedron around the V(II) site with the bonding axes of two hydrogens aligned nearly perpendicular to one another. Completion of the octahedron at the metal site brings both hydrogens inward in the coordination sphere, which is indicative of stronger binding interactions. In going from zero, to one, to two hydrogens bound, the V(II)−Cl distance changes from 2.30, to 2.33, to 2.39 Å. According to Kubas' classification, hydrogen complexes with the H−H distance in a range of 0.8−1.0 Å are classified as "true H_2 complexes" or, in other words, dihydrogen adducts.[40] Since the H−H distance of the H_2 molecule bound to the V(II)MFU-4*l* falls within this range, these complexes are best described as dihydrogen adducts. We further do not see substantial changes in the V−N benzotriazolate bond lengths, anticipating oxidative addition of H_2 to V(II) would be accompanied by shortening metal−ligand bonds.

To decompose metal−H_2 binding into physically meaningful interactions, we use Energy Decomposition Analysis (EDA), a tool based on Absolutely Localized Molecular Orbitals (ALMOs).[41−43] Here the MOF node and its ligated hydrogen(s) are partitioned into two interacting fragments. Separate single point calculations were performed on them followed by a block diagonal reassembly of MO coefficients to give the frozen density matrix and energy (ΔFrz). Polarization is described using a basis of fragment electric-field response functions (FERFs) which allows a fragment orbital to adjust to the weak electric field of its counterpart, resulting in dipolar and quadrupolar responses.[44] Finally, the charge transfer term ΔCT is computed from the difference between the completely relaxed and polarized electron density. The preparation energy (ΔPrep) is the energy required to distort the unbound MOF node and free hydrogen into their bound configuration. Δ*E* is the sum of all electronic contributions to binding, and Δ*H* evaluated at 77 K includes the effect of vibrations of nuclear modes at finite temperature. Columns I and II in Table 2 list the energy contributions Δ for single (V(II)-H_2) and double (V(II)H_2-H_2) loading, and Column III shows the changes ($\Delta\Delta = \Delta_2 - \Delta_1$) in each term for sequential ligation of the two hydrogens. Both hydrogens bind with charge transfer terms greater than 30 kJ/mol. Charge transfer was stronger for the second H_2 with a ΔΔ of −2.8 kJ/mol, along with a 2.0 kJ/mol increase in polarization interactions. Stronger short-range interactions on binding of the second H_2 are consistent with completion of the octahedral coordination sphere around vanadium(II) and counteract the reorganization energy (ΔΔPrep) required to bind the second H_2. Not only do we find two hydrogens bound strongly at the metal site, but the second equilvalent of H_2 binds 4.0 kJ/mol more strongly than binding for the first H_2. A negative ΔΔE that is largely driven by short-range interactions (charge transfer and polarization) shows that rearrangement at the binding site promotes ligation of the second hydrogen due to favorable orbital overlap, or in other words, the electronic binding energy of 2 hydrogens exhibits positive cooperativity.

The d^3 configuration in distorted square-pyramidal V(II) has been known to favor interactions with π acids for two reasons. First, the empty d_{z^2} orbital avoids potential antibonding σ^* interactions and enables close ligand approach. Second, a half filled d_π manifold is able to engage in backbonding where the effective range is shorter than that of the σ bond.[45,46] The pentacoordinate V(II) in MFU-4*l* is distorted trigonal bipyramidal (TBP) and transitions to a distorted octahedron on loading of the second hydrogen. To explore this further, we used a perturbative approach[41] to separate forward donation from backdonation. Donation from the hydrogen σ orbital to the empty metal d_{z^2} is the dominant charge transfer contributor, offering −23.4 and −26.1 kJ/mol of stabilization

https://doi.org/10.1021/acs.jpclett.2c02844
J. Phys. Chem. Lett. 2022, 13, 10471−10478

Table 1. Binding Energy and Its Decomposition for Ligation of Two Hydrogens to the V(II)MFU-4*l* Node Represented as the V(II)L_3X Cluster Model with L Standing for the Chelating Nitrogens of the Scorpionate SBU and X^- as the Placeholder for the Halide Counterion[a]

Fragments	X^-	ΔPrep	ΔFrz+Disp	ΔPol	ΔCT	ΔForw	ΔBack	Δ*E*
V(II)L_3X-H_2	F^-	6.7	8.6	−10.0	−28.4	−22.6	−5.8	−23.1
	Cl^-	8.8	19.8	−11.9	−30.1	−23.4	−6.6	−13.3
	Br^-	10.5	19.3	−11.9	−28.0	−22.5	−5.5	−10.1
	I^-	8.9	25.2	−13.9	−31.6	−25.6	−6.0	−11.5
V(II)L_3XH_2-H_2	F^-	9.1	12.2	−11.4	−29.2	−23.0	−6.2	−19.3
	Cl^-	11.1	18.3	−13.9	−32.8	−26.1	−6.7	−17.3
	Br^-	11.8	20.9	−15.5	−34.3	−28.0	−6.3	−17.1
	I^-	14.9	22.8	−17.2	−35.7	−29.4	−6.3	−15.3

[a]All contributions are in kJ/mol.

Table 2. Binding Energy, Enthalpy, and Free Energy at 77 K and 1 atm for H_2 Binding to V(II)XMFU-4*l*, X = F^-, Cl^-, Br^-, and I^-[a]

X^-	ΔE_1	ΔE_2	$\Delta\Delta E$	$\Delta H_1(T)$	$\Delta H_2(T)$	$\Delta\Delta H(T)$	$T\Delta S_1(T)$	$T\Delta S_2(T)$	$\Delta G_1(T)$	$\Delta G_2(T)$	$\Delta\Delta G(T)$
F^-	−23.1	−19.3	3.8	−19.3	−14.5	4.8	−7.1	−6.9	−12.2	−7.6	4.6
Cl^-	−13.3	−17.3	**−4.0**	−9.0	−10.3	**−1.3**	−7.0	−7.1	−2.0	−3.2	**−1.2**
Br^-	−10.1	−17.1	**−7.0**	−6.7	−9.3	**−2.6**	−7.0	−7.3	0.3	−2.0	**−2.3**
I^-	−11.5	−15.4	**−3.9**	−5.8	−7.6	**−1.8**	−7.1	−7.2	1.3	−0.5	**−1.8**

[a]ΔΔ values correspond to changes on second hydrogen loading ($\Delta_2 - \Delta_1$). All values are in kJ/mol.

for the first and second hydrogen loading. At shorter distances, favorable π overlap is afforded by the metal d_π backdonation to hydrogen σ^*, resulting in sizable contributions of −6.6 and −6.7 kJ/mol for binding the first and the second H_2. Strikingly, the presence of the first bound H_2 causes forward donation from the second H_2 to be strengthened with the backdonation remaining nearly identical.

Complementary occupied-virtual pairs (COVPs) constructed from unitary transformations within the occupied and virtual subspaces of the two fragments (the MOF node and hydrogen) provide a physical picture for orbitals engaged in forward bonding and backbonding. While the set of all COVPs exactly describes charge transfer between the fragments, the major energetic (and charge) contributions to bonding arise from one or two significant COVPs.[41] The charge transfer orbitals for V(II) to H_2 backbonding in Figure 2b plotted with an isodensity contour of 0.06 show the d_π orbitals of V(II) engaging with the hydrogen σ^* orbital. A closer inspection of the backdonating orbital at the MOF node reveals a contribution from the p_z orbital on the chloride ligand bound to V(II) (see Figure 2b). This motivated an investigation of the effect of halide substitution on the binding strength of hydrogen with the MOF node. Table 1 lists the binding energies for the sequential loading of two hydrogens onto the V(II)MFU-4*l* node represented as a V(II)L_3X complex containing an X^- halide bound to the metal. Among different halides, an F^- was found to promote the most favorable H_2 binding energies. Heavier halide ligands, especially in the case of Br^-, show strong comparative stabilization on binding the second H_2. This effect is driven by a stronger charge transfer term dominated by forward donation from H_2 to V(II). Thus, the halide ligand can be used to finely tune the strength of multiple H_2 binding with V(II) in this material.

Energy lowering upon H_2 binding is countered by the entropic tendency of the bound hydrogen to gain translational and rotational freedom. The free energy change on binding describes the balance between these two terms and determines the adsorption isotherm. We estimate the enthalpy and Gibbs free energy change of binding multiple hydrogens to the node with a standard frequency analysis at the B3LYP-D2/def2-SVP/RRHO level of theory and employ anharmonic 1D corrections to zero point vibrational energies (ZPVEs) for the frustrated modes of H_2. Low-frequency (≤100 cm^{-1}) normal modes were raised to 100 cm^{-1} for evaluation of the enthalpic and entropic terms to correct for the well-known breakdown of the harmonic oscillator model for soft vibrations.[47] The binding of each hydrogen adds 5 modes to the system due to the frustrated translations and rotation of bound H_2 on the MOF surface. Anharmonic 1D corrections to the ZPVEs of these modes were computed by employing the Fourier Grid Hamiltonian[48] to solve for the vibrational spectrum by sampling with a 1D potential energy surface (PES) with finite displacements around the equilibrium binding configuration under a frozen surface approximation. Details pertaining to anharmonic corrections to the ZPVE are included in Section I of the Supporting Information (SI). A scaling factor of s = 0.9893 obtained from quartic force fields was added to the B3LYP-D2 ZPVEs to account for anharmonic coupling between vibrational modes.[49]

Table 2 lists changes in binding energy, enthalpy, and free energies for the sequential binding of two hydrogens to V(II)MFU-4*l* at the temperature of liquid nitrogen (77 K) and 1 atm pressure. Thermal excitation of soft framework modes (<100 cm^{-1}) is dampened at such low temperatures, and the entropic penalty of binding is small compared to the enthalpy of binding. We employ a stoichiometric two-site model suggested by Dill and Bromberg[50] to predict binding isotherms. Hydrogen binds the V(II) center in the sequence $\langle V + H_2 \overset{K_1}{\rightarrow} V{-}H_2 + H_2 \overset{K_2}{\rightarrow} V{-}2H_2 \rangle$. The binding curve, determined by the average number of gas molecules $\nu = \langle i \rangle$ bound as a function of partial pressure p at temperature T, is given by

https://doi.org/10.1021/acs.jpclett.2c02844
J. Phys. Chem. Lett. 2022, 13, 10471−10478

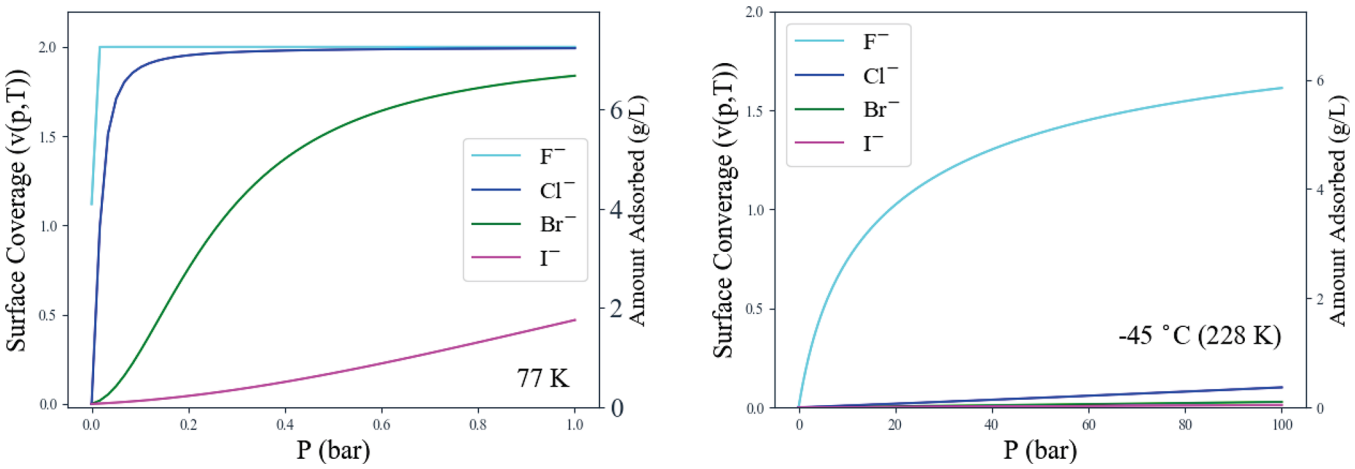

Figure 3. Predicted binding curve for halide variants of V(II)MFU-4*l* at 77 K, the temperature of liquid nitrogen (a, left), and at 228 K (−45 °C) (b, right).

Table 3. Binding Energy, Enthalpy, and Free Energy at 228 K (−45 °C) and 1 atm for H_2 Binding to V(II)XMFU-4*l*, X = F^-, Cl^-, Br^-, and I^-

X^-	ΔE_1	ΔE_2	$\Delta\Delta E$	$\Delta H_1(T)$	$\Delta H_2(T)$	$\Delta\Delta H(T)$	$T\Delta S_1(T)$	$T\Delta S_2(T)$	$\Delta G_1(T)$	$\Delta G_2(T)$	$\Delta\Delta G(T)$
F^-	−23.1	−19.3	3.8	−21.3	−16.3	5.0	−24.9	−23.9	3.6	7.5	4.0
Cl^-	−13.3	−17.3	**−4.0**	−10.6	−13.3	**−2.7**	−23.8	−26.4	13.2	13.1	**−0.1**
Br^-	−10.1	−17.1	**−7.0**	−8.4	−12.8	**−4.4**	−23.9	−27.7	15.6	14.8	**−0.7**
I^-	−11.5	−15.4	**−3.9**	−7.7	−11.6	**−4.0**	−24.7	−28.1	17.0	16.5	**−0.5**

$$v(p, T) = \frac{d \ln(Q)}{d \ln(p)},$$
$$\text{where } Q = 1 + K_1(T)p + K_1(T)K_2(T)p^2 \quad (1)$$

which is the binding polynomial that sums over the ligation states V, V−H_2, and V−2H_2. The equilibrium constants $K_i(T)$ were determined by the free energy of adsorption $\Delta G_i^\circ(T)$ at the standard pressure of 1 atm (1.01325 bar). Dimensionless surface coverage (θ) can be converted into measures for usable capacity by making use of crystallographic information. The MFU-4*l* unit cell is cubic with each edge L measuring 30.91 Å. A unit cell contains 8 nodes (n_N), each bearing 4 tetrahedral sites (n_o) that are capable of binding a maximum of two hydrogens (n_{H_2}). Assuming all tetrahedral sites in the node are transmetalated with V(II), the amount of hydrogen adsorbed with each site doubly occupied is given by $\frac{n_N \times n_o \times n_{H_2} \times m_{H_2}}{L^3}$ = 7.25 g/L. The smaller unit cell dimension (L = 21.63 Å) in MFU-4,[51] which contains the same type of nodes studied here, results in denser packing of metal sites and an increased maximum allowed hydrogen uptake of 21.18 g/L. While coupling between tetrahedral sites within a node that has multiple V(II) substitutions may impact the predicted binding curves, binding energies were found to lie in the range of −15 to −25 kJ/mol for nodes with V(II) substitutions at the adjacent tetrahedral sites (details in Table S1). Since H_2 is notably a weak-field ligand, one should not anticipate ligation of multiple H_2 molecules to cause significant changes in the overall spin-state. Metal−metal electronic communication has been demonstrated by M(tri)$_2$-type frameworks, which have a similar coordination environment around a metal site.[52] The benzotriazolate ligand has a π system, and if its π^* orbitals compete in energy with that of the occupied d orbitals at the metal sites, it could be possible that there is a ground state with ligand noninnocence, the investigation of which entails a scale of computations that were outside the purview of this particular work. (These estimates assume negligible changes in unit cell dimensions upon metal exchange of the parent Zn(II) material.) The secondary axis of binding curves in Figure 3 show predictions of total hydrogen uptake in g/L in V(II)MFU-4*l*. Since these predictions correspond to H_2 bound at the V sites and do not account for additional H_2 that will physisorb within the pore, they posit lower bounds for uptake. Advanced Grand Canonical Monte Carlo (GCMC) models for surface coverage such as the ones formulated by Snurr and co-workers[9,53] can be used to predict surface coverage due to dispersion interactions of H_2 with the pore that also takes into account other structural parameters of the MOF such as surface area and free volume. Strong uptake is seen at liquid nitrogen temperature at low pressures (0−1 bar) with almost all sites saturated by 0.5 bar for the F^- and Cl^- ligated node. The isotherm for the Br^- containing nodes shows sigmoidal shape with comparatively slower uptake in the low-pressure regime. The strongly negative $\Delta\Delta E$ for the Br^- containing node is attenuated when one considers the effect of ZPVEs and vibrational contributions to the enthalpy of and free energy of binding. Consequently, the binding isotherm at 77 K does not show a clear step on the ligation of the second H_2 (see Figure 3a). Weak binding in the iodide variant of MFU-4*l* results in a small percentage of sites being occupied. Open metal sites in MOFs that saturate after binding one H_2 would give overwhelmingly positive $\Delta\Delta H$ and $\Delta\Delta G$. Only the fluoride containing node shows a small positive $\Delta\Delta H(T)$ = 4.8 kJ/mol ($\Delta\Delta G$ = 4.6 kJ/mol). This node accommodates two hydrogens with strong binding enthalpies of $\Delta H_1(T)$ = −19.3 and $\Delta H_2(T)$ = −14.5 kJ/mol at liquid nitrogen temperatures. Consequently, the binding curves show a very steep uptake in the low-pressure (0−0.1 bar) range at 77 K.

https://doi.org/10.1021/acs.jpclett.2c02844
J. Phys. Chem. Lett. 2022, 13, 10471−10478

Cooling to cryogenic temperatures (−90 °C/183 K or lower) is expensive, and for practical applications of a nanoporous material one would want steep uptake at cool temperatures that are relatively inexpensive to access. In a recent technoeconomical analysis that looks at the potential of metal−organic frameworks for hydrogen backup power supply, it has been posited that cooling below −50 °C would incur significant costs.[54] Hence, we look at the binding curves at −45 °C (228 K), midway between the current DOE lower bound for operating temperature (−40 °C) and the temperature below which cooling becomes commercially unfeasible in Figure 3b. The corresponding energy, enthalpy, and free energy changes are reported in Table 3. V(II)FMFU-4*l* emerges with the steepest uptake for the 100−5 bar pressure swing. We estimate the usable capacity of the F^- containing V(II)MFU-4*l* node at 4.1 g/L at 228 K (Table 4). For the MFU-4 scaffold, which has a higher density of metal sites while retaining the same nodes, we predict a usable capacity of 11.9 g/L under these conditions. Interestingly, the predicted entropic penalty for binding the second hydrogen is greater when compared to that for the first for V(II)MFU-4*l* nodes containing heavier halides (Cl^-, Br^-, and I^-), which offsets the stronger electronic binding energy for ligation of the second H_2.

Table 4. Usable Capacity at 228 K (−45 °C) for the Fluoride Containing Node in MFU-4*l* and MFU-4 Assuming All Tetrahedral Sites in the Node Are Substituted With V(II) (n_o = 4)

	Amount Adsorbed (g/L)	
P (bar)	MFU-4*l*	MFU-4
5	1.8	5.2
100	5.8	17.1
Usable Capacity (g/L)	4.1	11.9

A key element in the materials design challenge for high-volumetric-density hydrogen storage in MOFs is the ability to reversibly bind multiple hydrogens at the first coordination sphere of a metal site. We predict that the V(II)MFU-4*l* node containing fluoride ligands can bind two hydrogen molecules per metal with binding enthalpies in the range of −15 to −25 kJ/mol. When compared to conventional open site metals in MOFs (e.g. Cu(I)MFU-4*l*), two H_2 binding to V(II) in V(II) exchanged MFU-4*l* doubles the volumetric capacity of the material at liquid nitrogen temperatures and offers strong uptake in the 100−5 bar pressure swing at −45 °C.

Consistent with the completion of octahedral coordination at the V(II) site, binding of the second hydrogen in the presence of the first is accompanied by an increase in charge transfer between the metal and hydrogen. Forward donation from H_2 to V(II) increases with the ligation of the second hydrogen to the node, with backdonation from the metal site remaining largely unchanged. Nodes containing heavier halides, especially Br^-, show stronger binding for ligation of the second hydrogen at the V(II), but this energy lowering is counteracted by a commensurate increase in the entropic penalty. Change in binding behavior with different halide ions in the node suggests that the anion coordinated to the binding site in this material can be used to finely tune the binding strength with H_2 or other guests. The MFU-4*l* parent scaffold, which has been shown to allow a broad range of metal substitutions at its tetrahedral metal sites, is critical in accommodating two hydrogens at the V(II) site. Provided the synthetic challenge of realizing a stable material with suitable density of V(II) sites is met, this strategy can be used to enable high-density H_2 storage at close to ambient temperatures of −45 °C. Thus, V(II)-MFU-4*l* and V(II)-MFU-4 represent promising candidate materials for the coordination of multiple H_2 molecules.

■ ASSOCIATED CONTENT

Supporting Information

The Supporting Information is available free of charge at https://pubs.acs.org/doi/10.1021/acs.jpclett.2c02844.

Further details pertaining to all computations and experiments performed, frustrated translational and rotational modes of bound H_2, and binding energy for the sequential ligation of two hydrogens indexed 1 and 2 (PDF)

Coordinates for all converged geometries. All electronic structure computations reported in this work were performed with the standard version of the Q-Chem 5.4 software package.[55] (ZIP)

Transparent Peer Review report available (PDF)

■ AUTHOR INFORMATION

Corresponding Authors

Romit Chakraborty − *Materials Sciences Division, Lawrence Berkeley National Laboratory, Berkeley, California 94720, United States; Department of Chemistry, University of California, Berkeley, California 94720, United States;* orcid.org/0000-0002-4638-6346; Email: romit@berkeley.edu

Martin Head-Gordon − *Materials Sciences Division and Chemical Sciences Division, Lawrence Berkeley National Laboratory, Berkeley, California 94720, United States; Department of Chemistry, University of California, Berkeley, California 94720, United States;* orcid.org/0000-0002-4309-6669; Email: mhg@cchem.berkeley.edu

Authors

Kurtis M. Carsch − *Materials Sciences Division, Lawrence Berkeley National Laboratory, Berkeley, California 94720, United States; Department of Chemistry, University of California, Berkeley, California 94720, United States;* orcid.org/0000-0003-4432-7518

David E. Jaramillo − *Materials Sciences Division, Lawrence Berkeley National Laboratory, Berkeley, California 94720, United States; Department of Chemistry, University of California, Berkeley, California 94720, United States;* orcid.org/0000-0002-3068-4963

Yuto Yabuuchi − *Materials Sciences Division, Lawrence Berkeley National Laboratory, Berkeley, California 94720, United States; Department of Chemistry, University of California, Berkeley, California 94720, United States;* orcid.org/0000-0003-3034-558X

Hiroyasu Furukawa − *Materials Sciences Division, Lawrence Berkeley National Laboratory, Berkeley, California 94720, United States; Department of Chemistry, University of California, Berkeley, California 94720, United States;* orcid.org/0000-0002-6082-1738

Jeffrey R. Long − *Materials Sciences Division and Chemical Sciences Division, Lawrence Berkeley National Laboratory, Berkeley, California 94720, United States; Department of*

https://doi.org/10.1021/acs.jpclett.2c02844
J. Phys. Chem. Lett. 2022, 13, 10471−10478

Chemistry, University of California, Berkeley, California 94720, United States; Department of Chemical and Biomedical Engineering, University of California, Berkeley, California 94720, United States; orcid.org/0000-0002-5324-1321

Complete contact information is available at: https://pubs.acs.org/10.1021/acs.jpclett.2c02844

Notes

The authors declare no competing financial interest.

■ ACKNOWLEDGMENTS

The authors gratefully acknowledge research support from the Hydrogen Materials - Advanced Research Consortium (HyMARC), established as part of the Energy Materials Network under the U.S. Department of Energy, Office of Energy Efficiency and Renewable Energy, under Contract No. DE-AC02-05CH11231. We wish to thank Jordan W. Taylor for providing the crystal structure for Zn(II)MFU-4*l*, Justin J. Talbot for help in compiling the table of contents figure, and James Shee and Benjamin E. R. Snyder for helpful comments.

■ REFERENCES

(1) Crabtree, G. W.; Dresselhaus, M. S.; Buchanan, M. V. The hydrogen economy. *Phys. Today* **2004**, *57*, 39−44.
(2) Armstrong, R. C.; Wolfram, C.; de Jong, K. P.; Gross, R.; Lewis, N. S.; Boardman, B.; Ragauskas, A. J.; Ehrhardt-Martinez, K.; Crabtree, G.; Ramana, M. The frontiers of energy. *Nat. Energy* **2016**, *1*, 15020.
(3) Sdanghi, G.; Maranzana, G.; Celzard, A.; Fierro, V. Review of the current technologies and performances of hydrogen compression for stationary and automotive applications. *Renew. Sust. Energy Rev.* **2019**, *102*, 150−170.
(4) Reddi, K.; Elgowainy, A.; Rustagi, N.; Gupta, E. Impact of hydrogen refueling configurations and market parameters on the refueling cost of hydrogen. *Int. J. Hydrog. Energy* **2017**, *42*, 21855−21865.
(5) Murray, L. J.; Dincă, M.; Long, J. R. Hydrogen storage in metal-organic frameworks. *Chem. Soc. Rev.* **2009**, *38*, 1294−1314.
(6) Suh, M. P.; Park, H. J.; Prasad, T. K.; Lim, D.-W. Hydrogen storage in metal-organic frameworks. *Chem. Rev.* **2012**, *112*, 782−835.
(7) Allendorf, M. D.; Hulvey, Z.; Gennett, T.; Ahmed, A.; Autrey, T.; Camp, J.; Cho, E. S.; Furukawa, H.; Haranczyk, M.; Head-Gordon, M.; et al. An assessment of strategies for the development of solid-state adsorbents for vehicular hydrogen storage. *Energy Environ. Sci.* **2018**, *11*, 2784−2812.
(8) Kapelewski, M. T.; Runčevski, T.; Tarver, J. D.; Jiang, H. Z.; Hurst, K. E.; Parilla, P. A.; Ayala, A.; Gennett, T.; Fitzgerald, S. A.; Brown, C. M.; Long, J. R. Record High Hydrogen Storage Capacity in the Metal−Organic Framework Ni_2(m-dobdc) at Near-Ambient Temperatures. *Chem. Mater.* **2018**, *30*, 8179−8189.
(9) Bae, Y. S.; Snurr, R. Q. Optimal isosteric heat of adsorption for hydrogen storage and delivery using metal−organic frameworks. *Microporous Mesoporous Mater.* **2010**, *132*, 300−303.
(10) Bueno-Pérez, R.; García-Pérez, E.; Gutiérrez-Sevillano, J. J.; Merkling, P. J.; Calero, S. A Simulation Study of Hydrogen in Metal−Organic Frameworks. *Adsorp. Sci. Technol.* **2010**, *28*, 823−835.
(11) Schneemann, A.; Wan, L. F.; Lipton, A. S.; Liu, Y. S.; Snider, J. L.; Baker, A. A.; Sugar, J. D.; Spataru, C. D.; Guo, J.; Autrey, T. S.; Jørgensen, M.; Jensen, T. R.; Wood, B. C.; Allendorf, M. D.; Stavila, V. Nanoconfinement of Molecular Magnesium Borohydride Captured in a Bipyridine-Functionalized Metal−Organic Framework. *ACS Nano* **2020**, *14*, 10294−10304.
(12) Schneemann, A.; White, J. L.; Kang, S.; Jeong, S.; Wan, L. F.; Cho, E. S.; Heo, T. W.; Prendergast, D.; Urban, J. J.; Wood, B. C.; Allendorf, M. D.; Stavila, V. Nanostructured Metal Hydrides for Hydrogen Storage. *Chem. Rev.* **2018**, *118*, 10775−10839.
(13) Tsivion, E.; Veccham, S. P.; Head-Gordon, M. High-Temperature Hydrogen Storage of Multiple Molecules: Theoretical Insights from Metalated Catechols. *ChemPhysChem* **2017**, *18*, 184−188.
(14) Sagara, T.; Klassen, J.; Ortony, J.; Ganz, E. Binding energies of hydrogen molecules to isoreticular metal-organic framework materials. *J. Chem. Phys.* **2005**, *123*, 014701.
(15) Runčevski, T.; Kapelewski, M. T.; Torres-Gavosto, R. M.; Tarver, J. D.; Brown, C. M.; Long, J. R. Adsorption of two gas molecules at a single metal site in a metal-organic framework. *ChemComm* **2016**, *52*, 8251−8254.
(16) Tachikawa, H.; Iyama, T. Mechanism of hydrogen storage in the graphene nanoflake-lithium-H2 system. *J. Phys. Chem. C* **2019**, *123*, 8709−8716.
(17) Jaramillo, D. E.; Jiang, H. Z.; Evans, H. A.; Chakraborty, R.; Furukawa, H.; Brown, C. M.; Head-Gordon, M.; Long, J. R. Ambient-Temperature Hydrogen Storage via Vanadium (II)-Dihydrogen Complexation in a Metal−Organic Framework. *J. Am. Chem. Soc.* **2021**, *143*, 6248−6256.
(18) Comito, R. J.; Wu, Z.; Zhang, G.; Lawrence, J. A.; Korzyński, M. D.; Kehl, J. A.; Miller, J. T.; Dincă, M. Stabilized Vanadium Catalyst for Olefin Polymerization by Site Isolation in a Metal−Organic Framework. *Angew. Chem., Int. Ed.* **2018**, *57*, 8135−8139.
(19) Oppenheim, J. J.; Mancuso, J. L.; Wright, A. M.; Rieth, A. J.; Hendon, C. H.; Dinca, M. Divergent Adsorption Behavior Controlled by Primary Coordination Sphere Anions in the Metal−Organic Framework Ni_2X_2BTDD. *J. Am. Chem. Soc.* **2021**, *143*, 16343−16347.
(20) Biswas, S.; Grzywa, M.; Nayek, H. P.; Dehnen, S.; Senkovska, I.; Kaskel, S.; Volkmer, D. A cubic coordination framework constructed from benzobistriazolate ligands and zinc ions having selective gas sorption properties. *Dalton Trans.* **2009**, 6487−6495.
(21) Schmieder, P.; Denysenko, D.; Grzywa, M.; Baumgärtner, B.; Senkovska, I.; Kaskel, S.; Sastre, G.; van Wüllen, L.; Volkmer, D. CFA-1: the first chiral metal-organic framework containing Kuratowski-type secondary building units. *Dalton Trans.* **2013**, *42*, 10786−10797.
(22) Trofimenko, S. Recent advances in poly(pyrazolyl)borate (scorpionate) chemistry. *Chem. Rev.* **1993**, *93*, 943−980.
(23) Dubey, R. J.; Comito, R. J.; Wu, Z.; Zhang, G.; Rieth, A. J.; Hendon, C. H.; Miller, J. T.; Dinca, M. Highly Stereoselective Heterogeneous Diene Polymerization by Co-MFU-4l: A Single-Site Catalyst Prepared by Cation Exchange. *J. Am. Chem. Soc.* **2017**, *139*, 12664−12669.
(24) Denysenko, D.; Grzywa, M.; Jelic, J.; Reuter, K.; Volkmer, D. Scorpionate-Type Coordination in MFU-4l Metal−Organic Frameworks: Small-Molecule Binding and Activation upon the Thermally Activated Formation of Open Metal Sites. *Angew. Chem., Int. Ed.* **2014**, *53*, 5832−5836.
(25) Metzger, E. D.; Comito, R. J.; Hendon, C. H.; Dincă, M. Mechanism of single-site molecule-like catalytic ethylene dimerization in Ni-MFU-4l. *J. Am. Chem. Soc.* **2017**, *139*, 757−762.
(26) Comito, R. J.; Metzger, E. D.; Wu, Z.; Zhang, G.; Hendon, C. H.; Miller, J. T.; Dincă, M. Selective Dimerization of Propylene with Ni-MFU-4l. *Organometallics* **2017**, *36*, 1681−1683.
(27) Mardirossian, N.; Head-Gordon, M. ωB97M-V: A combinatorially optimized, range-separated hybrid, meta-GGA density functional with VV10 nonlocal correlation. *J. Chem. Phys.* **2016**, *144*, 214110.
(28) Vydrov, O. A.; van Voorhis, T. Nonlocal van der Waals density functional: The simpler the better. *J. Chem. Phys.* **2010**, *133*, 244103.
(29) Mardirossian, N.; Head-Gordon, M. Thirty years of density functional theory in computational chemistry: an overview and extensive assessment of 200 density functionals. *Mol. Phys.* **2017**, *115*, 2315−2372.
(30) Goerigk, L.; Hansen, A.; Bauer, C.; Ehrlich, S.; Najibi, A.; Grimme, S. A look at the density functional theory zoo with the advanced GMTKN55 database for general main group thermochemistry, kinetics and noncovalent interactions. *Phys. Chem. Chem. Phys.* **2017**, *19*, 32184−32215.

(31) Najibi, A.; Goerigk, L. The Nonlocal Kernel in van der Waals Density Functionals as an Additive Correction: An Extensive Analysis with Special Emphasis on the B97M-V and omega B97M-V Approaches. *J. Chem. Theory Comput.* **2018**, *14*, 5725−5738.
(32) Santra, G.; Martin, J. M. L. Some observations on the performance of the most recent exchange-correlation functionals for the large and chemically diverse GMTKN55 benchmark. *AIP Conf. Proc.* **2019**, *2186*, 030004.
(33) Chan, B.; Gill, P. M. W.; Kimura, M. Assessment of DFT Methods for Transition Metals with the TMC151 Compilation of Data Sets and Comparison with Accuracies for Main-Group Chemistry. *J. Chem. Theory Comput.* **2019**, *15*, 3610−3622.
(34) Veccham, S. P.; Head-Gordon, M. Density Functionals for Hydrogen Storage: Defining the H2Bind195 Test Set with Ab Initio Benchmarks and Assessment of 55 Functionals. *J. Chem. Theory Comput.* **2020**, *16*, 4963−4982.
(35) Veccham, S. P.; Head-Gordon, M. Assessment of Performance of Density Functionals for Predicting Potential Energy Curves in Hydrogen Storage Applications. *J. Phys. Chem. A* **2021**, *125*, 4245−4257.
(36) Sure, R.; Grimme, S. Corrected small basis set Hartree-Fock method for large systems. *J. Comput. Chem.* **2013**, *34*, 1672−1685.
(37) Weigend, F.; Ahlrichs, R. Balanced basis sets of split valence, triple zeta valence and quadruple zeta valence quality for H to Rn: Design and assessment of accuracy. *Phys. Chem. Chem. Phys.* **2005**, *7*, 3297−3305.
(38) Rappoport, D.; Furche, F. Property-optimized Gaussian basis sets for molecular response calculations. *J. Chem. Phys.* **2010**, *133*, 134105.
(39) Boys, S. F.; Bernardi, F. The calculation of small molecular interactions by the differences of separate total energies. Some procedures with reduced errors. *Mol. Phys.* **1970**, *19*, 553−566.
(40) Kubas, G. J. Fundamentals of H2 binding and reactivity on transition metals underlying hydrogenase function and H 2 production and storage. *Chem. Rev.* **2007**, *107*, 4152−4205.
(41) Khaliullin, R. Z.; Cobar, E. A.; Lochan, R. C.; Bell, A. T.; Head-Gordon, M. Unravelling the origin of intermolecular interactions using absolutely localized molecular orbitals. *J. Phys. Chem. A* **2007**, *111*, 8753−8765.
(42) Horn, P. R.; Mao, Y.; Head-Gordon, M. Probing non-covalent interactions with a second generation energy decomposition analysis using absolutely localized molecular orbitals. *Phys. Chem. Chem. Phys.* **2016**, *18*, 23067−23079.
(43) Levine, D. S.; Head-Gordon, M. Energy decomposition analysis of single bonds within Kohn-Sham density functional theory. *Proc. Natl. Acad. Sci. U.S.A* **2017**, *114*, 12649−12656.
(44) Horn, P. R.; Head-Gordon, M. Polarization contributions to intermolecular interactions revisited with fragment electric-field response functions. *J. Chem. Phys.* **2015**, *143*, 114111.
(45) Lee, K.; et al. Design of a metal-organic framework with enhanced back bonding for separation of N_2 and CH_4. *J. Am. Chem. Soc.* **2014**, *136*, 698−704.
(46) Lee, K.; Howe, J. D.; Lin, L. C.; Smit, B.; Neaton, J. B. Small-molecule adsorption in open-site metal-organic frameworks: A systematic density functional theory study for rational design. *Chem. Mater.* **2015**, *27*, 668−678.
(47) Ribeiro, R. F.; Marenich, A. V.; Cramer, C. J.; Truhlar, D. G. Use of solution-phase vibrational frequencies in continuum models for the free energy of solvation. *J. Phys. Chem. B* **2011**, *115*, 14556−14562.
(48) Clay Marston, C.; Balint-Kurti, G. G. The Fourier grid Hamiltonian method for bound state eigenvalues and eigenfunctions. *J. Chem. Phys.* **1989**, *91*, 3571−3576.
(49) Kesharwani, M. K.; Brauer, B.; Martin, J. M. Frequency and zero-point vibrational energy scale factors for double-hybrid density functionals (and other selected methods): Can anharmonic force fields be avoided? *J. Phys. Chem. A* **2015**, *119*, 1701−1714.
(50) Dill, K. A.; Bromberg, S.; Stigter, D.*Molecular Driving Forces: Statistical Thermodynamics In Biology, Chemistry, Physics, and Nanoscience*; Garland Science: London and New York, 2010; p 563.
(51) Denysenko, D.; Grzywa, M.; Tonigold, M.; Streppel, B.; Krkljus, I.; Hirscher, M.; Mugnaioli, E.; Kolb, U.; Hanss, J.; Volkmer, D. Elucidating gating effects for hydrogen sorption in MFU-4-type triazolate-based metal-organic frameworks featuring different pore sizes. *Chem.—Eur. J.* **2011**, *17*, 1837−1848.
(52) Park, J. G.; Collins, B. A.; Darago, L. E.; Runčevski, T.; Ziebel, M. E.; Aubrey, M. L.; Jiang, H. Z.; Velasquez, E.; Green, M. A.; Goodpaster, J. D.; Long, J. R. Magnetic ordering through itinerant ferromagnetism in a metal-organic framework. *Nat. Chem.* **2021**, *13*, 594−598.
(53) Frost, H.; Snurr, R. Q. Design requirements for metal-organic frameworks as hydrogen storage materials. *J. Phys. Chem. C* **2007**, *111*, 18794−18803.
(54) Peng, P.; Anastasopoulou, A.; Brooks, K.; Furukawa, H.; Bowden, M. E.; Long, J. R.; Autrey, T.; Breunig, H. Cost and potential of metal-organic frameworks for hydrogen back-up power supply. *Nat. Energy* **2022**, *7*, 448−458.
(55) Epifanovsky, E.; Gilbert, A. T.; Feng, X.; Lee, J.; Mao, Y.; Mardirossian, N.; Pokhilko, P.; White, A. F.; Coons, M. P.; Dempwolff, A. L.; et al. Software for the frontiers of quantum chemistry: An overview of developments in the Q-Chem 5 package. *J. Chem. Phys.* **2021**, *155*, 084801.

https://doi.org/10.1021/acs.jpclett.2c02844
J. Phys. Chem. Lett. 2022, 13, 10471−10478